A new constitutive model for cutting simulation of 316L austenitic stainless steel

Available online at www.sciencedirect.com

ScienceDirect

Procedia CIRP 82 (2019) 53–58

www.elsevier.com/locate/procedia

17th CIRP Conference on Modelling of Machining Operations

A new constitutive model for cutting simulation of 316L austenitic stainless steel

Amir Malakizadi[a,b,*], Jannick Nils Oberbeck[a], Martin Magnevall[b], Peter Krajnik[a]

[a]*Chalmers University of Technology, Gohenburg, SE- 412 96, Sweden*
[b]*Sandvik Coromant, Sandviken SE-811 81, Sweden*

* Corresponding author. Tel.: +46-31-7726377. *E-mail address:* amir.malakizadi@chalmers.se

Abstract

In this study, a new phenomenological model is proposed to describe the flow stress properties of 316L austenitic stainless steel at high strains strain rates and temperatures encountered in metal cutting. Additionally, a novel approach is presented for calibration of the proposed model which combines the experimental flow stress data with inverse modelling of the orthogonal cutting process. The simulation results including the cutting forces and chip shapes are compared with the experimental results attained using tailored tools with different rake angles. This model showed improved prediction capabilities in comparison with those obtained from the widely used Johnson-Cook material model.

Peer-review under responsibility of the scientific committee of The 17th CIRP Conference on Modelling of Machining Operations

Keywords: Stainless steel; Cutting; Calibration; Inverse identification

1. Introduction

The Finite Element (FE) simulation of the cutting process has growingly become an imperative step for research and development in the field during the last decades. The main areas of industrial importance include the simulation of cutting forces and temperature, tool wear, residual stresses and the surface microstructure influencing the ultimate performance of the machined parts [1]. However, it is shown that the reliability of the FE simulation results depends largely on the physical and numerical assumptions in connection , for example, with the thermo-mechanical coupling and friction/contact definition at the tool-chip interface as well as with the constitutive and damage models [2].

Implementation of the proper constitutive and damage models – to describe the flow stress behaviour and failure response of the work materials under the extreme conditions encountered in the cutting process – proved to have a significant effect on the reliability of FE simulation results. Thus, a vast number of studies have been dedicated to the model derivations and the advanced methodologies for calibration of constitutive parameters under the relevant range of strain, strain rate and temperature. These attempts are generally led to the development of two main different types of constitutive models: (1) phenomenological models such as Johnson-Cook (JC) [3] and its modifications [4, 5] and (2) the physics-based relations such as Zerilli-Armstrong [6] model and the more recent models by Svoboda et al. [7] and Liu et al. [8, 9]. The main reason for popularity of the phenomenological models lies in their simplicity and availability in FE commercial codes. On the other hand, the physics-based models can, provide more reliable predictions and they may offer additional insights into the machined surface properties such as the hardness, grain size distribution, dislocation density resulted from severe material deformations. However, a drawback of the physics-based constitutive relations is the large number of input data required for the model calibration. Moreover, they are often computationally costlier than the phenomenological models. These factors have therefore limited the application of physics-based constitutive models for cutting simulations.

Johnson-Cook (JC) material model is one of the most widely used relations for cutting process simulations, mainly because

2212-8271
Peer-review under responsibility of the scientific committee of The 17th CIRP Conference on Modelling of Machining Operations
10.1016/j.procir.2019.04.064

(1) it is available in most FE codes such as ABAQUS, DEFORM 2D/3D, AdvantEdge and MSC-Marc and (2) the flow stress parameters are available for a large number of ferrous and non-ferrous alloys. It is however showed that the JC model does not properly represent the strain and strain rate hardening and thermal softening behaviours of specific alloys. Hence, several modifications have been made to improve its prediction capabilities. For example, Karpat [4] proposed a phenomenological constitutive model to adopt the effects of dynamic recrystallisation (DRX) and dynamic recovery (DRV) on the shear planes when machining Ti-6Al-4V. Sima and Özel [5] have developed similar types of model but with an improved strain softening behaviour. Malakizadi et al. [10] implemented a modified JC model with improved thermal softening and strain rate hardening responses for cutting simulations of 20MnCrS5 case hardening steel.

In this study, we propose a new constitutive model with eight material parameters to simulate the flow stress behaviour of 316L austenitic stainless steel during cutting process. A novel approach is presented for the model calibration under a wide range of strain, strain rate and temperature encountered in the cutting zone. The FE simulation results in terms of the cutting forces and the chip shape parameters are compared with experimental data at two different conditions. Additionally, the model predictions were compared with the JC material model.

2. Material analysis and cutting experiments

The microstructural and hardness properties of the 316L austenitic stainless steel cylindrical bar (Φ150mm) were investigated prior to the cutting experiments. The samples were taken from the bar and close to the surface within the range of diameter where the grooves were made in the next step for the orthogonal cutting tests. A FEI/Philips XL-30 and a LEO 1550 Gemini SEM were used for microstructural analysis after the proper sample preparations. The grain size was measured based on the mean lineal intercept method. The Vickers hardness test was performed on the as-polished surfaces using 10 kgf indentation load (HV10). At least five measurements were done on the sample. The analysis showed an average grain size of about 36 µm and an average hardness of 155 HV10.

A workpiece was prepared from the same bar for the orthogonal cutting tests. Several flanges with 3mm width were initially fabricated by grooving inserts. These flanges were then machined in the radial direction to meet the orthogonality and plane strain conditions. Prior to the cutting tests, several TCMW16T304 uncoated cemented carbide inserts (H13A Sandvik Coromant grade) with 0° and 7° rake and clearance angles were ground to make cutting edges with ±10 rake angles. A STFCL2020K16 tool holder with 91° cutting edge angle was used for cutting experiments. Machining tests were performed under dry condition at cutting speed (V_C) of 200 m/min and feed rate (f) of 0.16 mm/rev. Each test was repeated twice and the cutting forces were measured using a Kistler 9263A three component dynamometer. The cutting time was kept constant (5s) for all the tests. The tools were sliced approximately from the middle of the tool-chip contact region width using a diamond blade and mounted for further analyses.

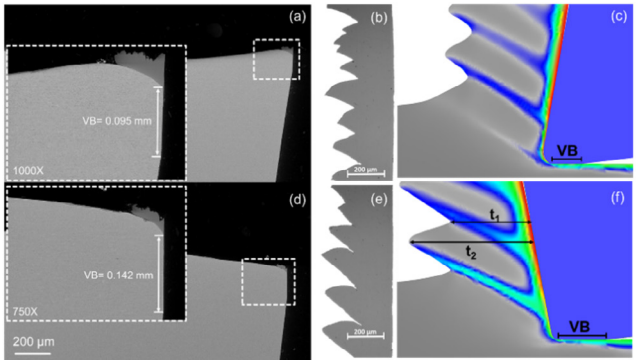

Fig. 1: (a and d) The cross-section of the tools indicating the flank wear land after 5s machining time and when using the positive and negative rake angles, (b and e) the serrated chip formation resulted by the tools with the respective rake angles. (c and f) the representation of the worn tool geometries used in FE simulation of the cutting process.

The cross-section of the tool was then examined using SEM to measure the flank wear land widths (VB), see Figs.1a and 1d. The respective values of the wear land widths were used to model the tool geometries required for cutting simulations as shown in Figs.1c and 1f. Since the worn geometry of the tool affects the cutting and feed forces, only the measured values during the last 0.1s of the cuts were extracted to compare with simulation results. Finally, the chip shape parameters, t_1 and t_2 shown in Fig. 1f, were measured after mounting and polishing the collected chips.

3. Finite Element modelling

DEFORM 2D commercial software was used for cutting simulations in this study. The worn geometry of the cutting tools was prepared in CATIA modelling software and transferred with the IGES format into the DEFORM 2D environment. The tool was assumed rigid, but it allows heat transfer during the simulations. The element size in the tool was restricted to 7 µm near the cutting edge using the mesh window technique. The same method was used to define the element size near the cutting zone and along the shear planes in the work material (7µm). The work material was assumed elasto-viscoplastic and the Lagrangian incremental FE formulation was used for the cutting simulations. JC material model was used to describe the flow stress properties as a reference model:

$$\sigma = (A + B\varepsilon^n)\left(1 + C\ln\left(\frac{\dot{\varepsilon}}{\dot{\varepsilon}_0}\right)\right)\left(1 - \left(\frac{T-T_r}{T_m-T_r}\right)^m\right) \quad (1)$$

where A, B, C, n and m are the material parameters and $\dot{\varepsilon}_0$ is the reference strain rate. T, T_m and T_r are the temperature, melting point and the room temperature, respectively.

The constitutive model proposed in the current study provides an additional strain softening effect as well as an improved thermal softening behaviour compared to the widely used JC material model (Eq. 1). With these additional factors, this model can provide the flow stress properties of 316L

austenitic stainless steel within a larger range of strain, strain rate and temperature encountered in the cutting zone:

$$\sigma = \left(A + B\varepsilon^{n_1}\left(\frac{1}{\exp(n_2\varepsilon)}\right)\right)\left(1 + C\ln\left(\frac{\dot{\varepsilon}}{\dot{\varepsilon}_0}\right)\right) f(T) \quad (2)$$

where *f(T)* is the thermal softening function, given as:

$$f(T) = \left(1 - \exp\left(\lambda_1 - \lambda_2\left(\frac{T}{T_m}\right)^{\lambda_3}\right)\right) \quad (3)$$

A, B, C, n_1, n_2, λ_1, λ_2 and λ_3 are the eight material parameters and $\dot{\varepsilon}_0$ is the reference strain rate. T and T_m are the temperature, melting point, respectively.

The modified Cockcroft-Latham (CL) fracture criterion was used to estimate the initiation point for the material failure at primary shear zone:

$$W_{CL} = \int_0^t \sigma^* \dot{\varepsilon}_p dt \quad \text{where} \quad \sigma^* = \begin{cases} \sigma^* = \sigma_e & \sigma_1 > 0 \\ \sigma^* = 0 & \sigma_1 < 0 \end{cases} \quad (4)$$

σ_e and σ_1 in Eq. 4 are the equivalent von Mises and first principal stresses, respectively. $\dot{\varepsilon}_p$ is the equivalent plastic strain. This damage criterion was implemented using a Fortran subroutine in the DEFORM 2D environment. Once the fracture initiation parameter, W_{CL}, exceeds during the chip formation process, the flow stress of the respective element instantaneously reduces by a predefined factor (δ) as shown in Fig. 2.

A pressure dependent shear friction model was implemented to simulate the frictional condition at the tool-chip interface:

$$\tau_f = [1 - \exp(-\alpha_1 {\sigma_n}^{\alpha_2})]k \quad (5)$$

This model was also implemented in DEFORM 2D using a Fortran subroutine. In Eq. 5, τ_f and σ_n are the shear and the normal stresses acting on the tool rake and flank surfaces and k is the shear strength of work material estimated by Eq. 1 or Eq. 2. α_1 and α_2 are the model constants, assumed 0.012 and 1, respectively. A perfect thermal condition was assumed between the tool, chip and work materials, by defining a large heat transfer coefficient of h = 10^5 kW/m^2°C for the respective surfaces. The viability of the adopted thermal and frictional boundary conditions was discussed in detail in previous investigations [11, 12]. Table 1 summarizes the thermal and elastic properties of 316L stainless steel obtained using JMatPro® material modelling software and the physical properties of H13A tool material used in the present study.

Table 1. Thermal and elastic properties of 316L (upper part) and H13A tool (lower part) materials.

Property	Equation
Heat capacity (J/cm^3°C)	$1.135 \times 10^{-3}T + 3.62$
Thermal conductivity (W/m°C)	$1.313 \times 10^{-2}T + 13.89$
Elastic Modulus (GPa)	$-0.0752T + 194.55$
Poisson ratio (-)	$4.527 \times 10^{-5}T + 0.296$
Heat capacity (J/cm^3°C)	$3 \times 10^{-9}T^3 - 5 \times 10^{-6}T^2 + 0.0041T + 2.8857$
Thermal conductivity (W/m°C)	$-2 \times 10^{-10}T^4 + 4 \times 10^{-7}T^3 - 0.0003T^2 + 0.0419T + 2.8857$

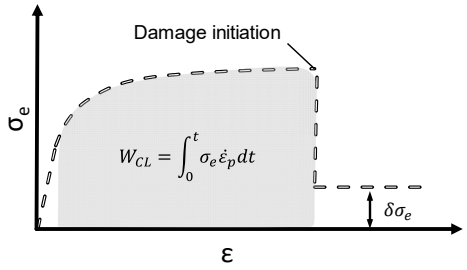

Fig. 2: The Cockcroft-Latham fracture criterion and damage softening.

4. Calibration of constitutive and damage parameters

The proposed constitutive (Eq. 2) was calibrated in three steps shown in Fig. 3 to describe the flow stress behaviour of the work material within a wide range of strain, strain rate and temperature that occur in cutting zone.

The first step was to determine the thermal softening parameters given in Eq. 3. This was done using the flow stress data reported by Wedberg and Lindgren [13], see Fig. 4a. Here, the flow stress data at the strain rate of 0.01 s^{-1} was used for the calibration of the thermal softening parameters. Hence, this value was assumed as the reference strain rate, $\dot{\varepsilon}_0$, in Eq. 2. The flow stress values at the available temperatures were normalized with respect to the room temperature data at three different levels of strain: 0.3, 0.4 and 0.5. The results were then plotted for the respective temperatures as shown in Fig. 5. The results in Figs. 4 and 5 show a significant thermal softening response nearly above 800-850°C. A similar behaviour was also predicted by JMatPro® material software [14], as shown in Fig. 5. Therefore, two sets of parameters are to be obtained for thermal softening behaviour of 316L below and above 800 °C. This was done by minimizing the following at two ranges of temperature: 0-800°C and 800-1350°C according to

$$\text{Min}\big(F(\boldsymbol{X})\big) \text{ subjected to } -10 \le \boldsymbol{X} \le 10$$
$$\text{where:} \quad F(\boldsymbol{X}) = \frac{1}{2}\sum_{i=1}^{N}(g_i(\boldsymbol{X}) - \bar{g}_i)^2 \quad (6)$$

Here, $\boldsymbol{X}$ is a vector including the softening parameters: λ_1, λ_2 and λ_3. g_i is the thermal softening response according to Eq. 3 for a given temperature and the input vector $\boldsymbol{X}$. $\bar{g}_i$ is the experimental thermal softening values at given temperature and strain. The multi-start interior point optimization method in MATLAB® with 20 initial points was used to determine the global optimum within the specified limits.

The second step involved the calibration of strain hardening and strain softening parameters: A, B, n_1 and n_2. The aim here is to determine the optimum set of material parameters using the available flow stress data provided at the reference strain rate but at different temperatures up to 900°C, see Fig. 4a. The thermal softening parameters obtained in the first step were set fixed and the strain hardening and strain softening parameters in Eq. 2 were determined using a similar minimization method described in Eq. 6. Here, g_i and $\bar{g}_i$ represent two vectors including the simulated and experimental stress values for a given temperature. Different upper limits between 0 and 0.5 were set for the strain softening parameter during minimization, whereas $A, B, n_1 \ge 0$ was the only constraint set for strain hardening parameters.

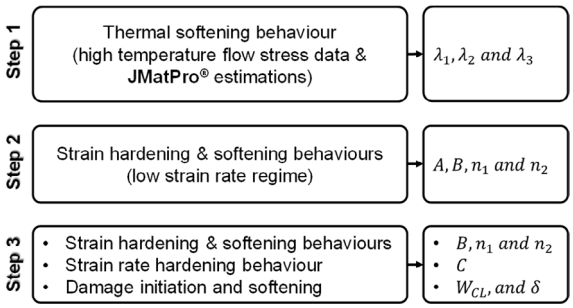

Fig. 3: The steps used for calibration of the proposed constitutive model.

As evident in Fig. 4b, different sets of parameters resulted in a similar response at low range of strains; however, the strain softening behaviour varied significantly at larger range of strains, more relevant to the cutting process. Thus, the last step involved an inverse approach to determine the optimum set of strain hardening and strain softening parameters along with the strain rate hardening and damage parameters. This approach combines Response Surface Methodology and Finite Element modelling of the orthogonal cutting process for calibration of the material parameters. A detailed description of this approach is given in [12]. Here, different combinations of material and damage parameters including B, n_1, n_2, C and W_{CL} were generated using Central Composite Design (CCD) to obtain the response surfaces for the simulated cutting and feed forces and chip shape parameters: t_1 and t_2. Preliminary FE analyses indicated that the effect of the damage softening parameter (δ) and the damage initiation criterion (W_{CL}) on the chip shapes and the forces is nearly the same. Thus, δ was assumed constant at 30% and only W_{CL} was considered for the design of experiment. Moreover, A, λ_1, λ_2 and λ_3 determined in steps 1 and 2 were kept constant for all FE simulations.

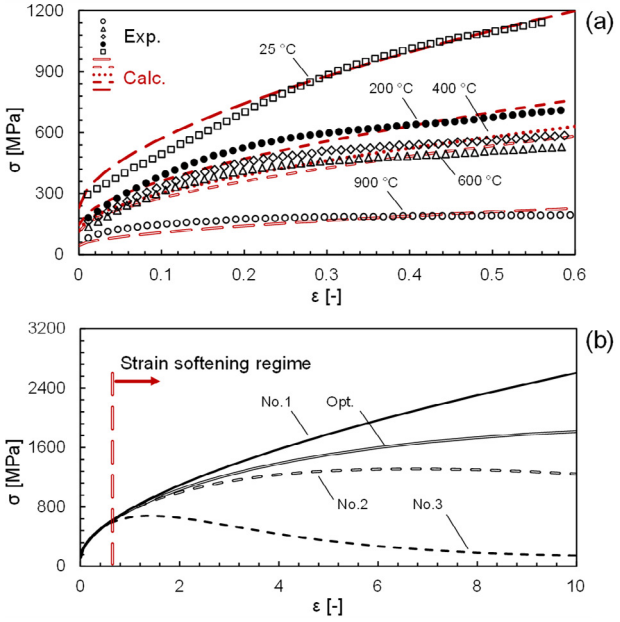

Fig. 4: (a) The experimental flow stress responses for 316L austenitic stainless steel at various temperatures and constant strain rate of 0.01 s^{-1} along with the calculated curves (b) the estimated flow stress response at T = 500°C and $\dot{\varepsilon} = 0.01$ s^{-1} for different combinations of B, n_1 and n_2 in the Eq. 2.

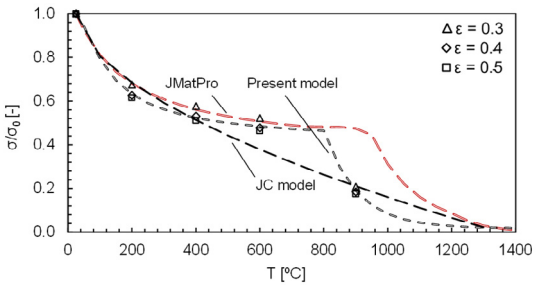

Fig. 5: Thermal softening behaviour of 316L and the estimations by JC model, JMatPro® material software and the calibrated constative model presented in this study.

A MATLAB® code was developed to generate the tabulated flow stress data at different ranges of strain (up to 20), strain rate (up to 10^5 s^{-1}) and temperature (up to 1300 °C). The tabulated data and the damage initiation criterion were written in the KEY files and databases were generated for each of 27 combinations of material inputs generated by CCD. The FE simulation results of interest were then extracted from the models and the second-order response surfaces were determined using regression analysis [12]. The final step involved identification of the material parameters by minimizing the difference between the response surfaces and the corresponding experimental measurements at the given cutting condition: V_C = 200 m/min and f = 0.16 mm/rev:

$$\text{Min}\big(F(\boldsymbol{X})\big) \text{ subjected to } \boldsymbol{x_L} \le \boldsymbol{X} \le \boldsymbol{x_U}$$

$$\text{where:} \quad F(\boldsymbol{X}) = \sum_{i=1}^{4}\left[w_i\left(\frac{y_i(X)-\overline{y_i}}{\overline{y_i}}\right)^2\right] \qquad (7)$$

Here, $\boldsymbol{X}$ is a vector including B, n_1, n_2, C and W_{CL} material parameters and w_i represents the weight factors for each response of interest in the minimization problem. y_i is the simulated response (e.g. cutting force) for a given set of material parameters, $\boldsymbol{X}$, and $\overline{y_i}$ is the corresponding experimental result. $\boldsymbol{x_L}$ and $\boldsymbol{x_U}$ are two vectors representing the boundaries set for the generated material parameters based on CCD. A similar optimization algorithm as the steps 1 and 2 was used here.

Table 2. Material parameters for JC and the presented constitutive model. *n = 0.61, **m = 0.517 for JC model [15].

Model and parameters		A	B	C	n_1	n_2
No. 1	T< 800°C T> 800°C	230	1309	0.052 0.180	0.58	0
No. 2	T< 800°C T> 800°C	230	1397	0.060 0.180	0.60	0.09
No. 3	T< 800°C T> 800°C	230	1800	0.060 0.180	0.70	0.50
Opt.	T< 800°C T> 800°C	230	1334	0.060 0.180	0.58	0.04
JC		305	1161	0.010	0.61*	–
		λ_1	λ_2	λ_3	W_{CL}	$\dot{\varepsilon}_0$
No. 1	T< 800°C T> 800°C	-0.527 -0.016	0.053 0.004	-1.144 -9.562	1100	0.01
No. 2	T< 800°C T> 800°C	-0.527 -0.016	0.053 0.004	-1.144 -9.562	1100	0.01
No. 3	T< 800°C T> 800°C	-0.527 -0.016	0.053 0.004	-1.144 -9.562	1200	0.01
Opt.	T< 800°C T> 800°C	-0.527 -0.016	0.053 0.004	-1.144 -9.562	800	0.01
JC		0.517**	–	–	800	1

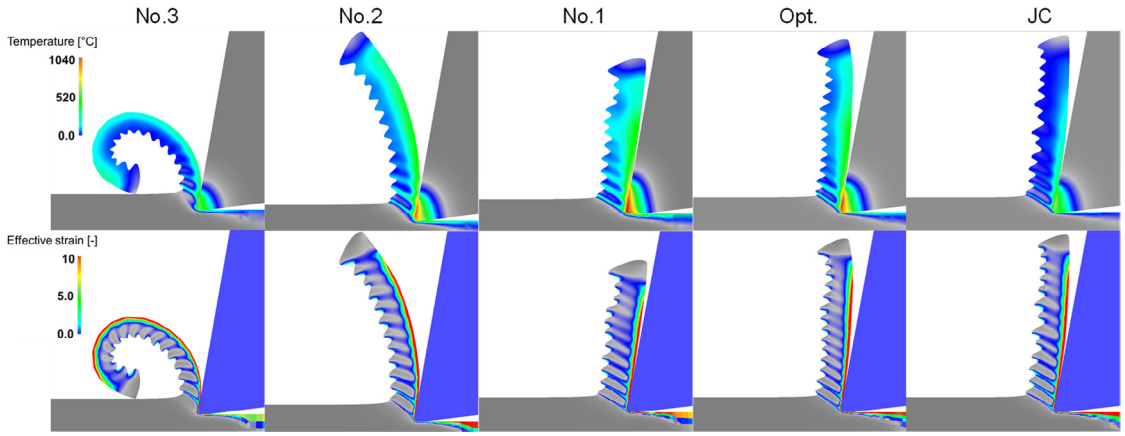

Fig. 6: The FE simulation results (temperature and effective strain) using different combinations of material parameters given in Table 2. V_C = 200 m/min, f = 0.016 mm/rev, 10° rake angle, VB = 0.095 mm.

Table 2 summarizes the different sets of material parameters for the proposed constitutive model (Eq. 2) shown in the flow stress plots in Fig. 4b. The JC material parameters reported by Chandrasekaran et al. [15] are also given in Table 2.

5. Results and discussion

The comparison between the FE simulation results of temperature and effective strain, incorporating the material data given in Table 2 for the JC model (Eq. 1) and the constitutive model presented in the current study (Eq. 2), is shown in Fig. 6. Evidently, the JC material model resulted in nearly the same chip formation compared to the case where the optimum set of parameters was used in Eq. 2.

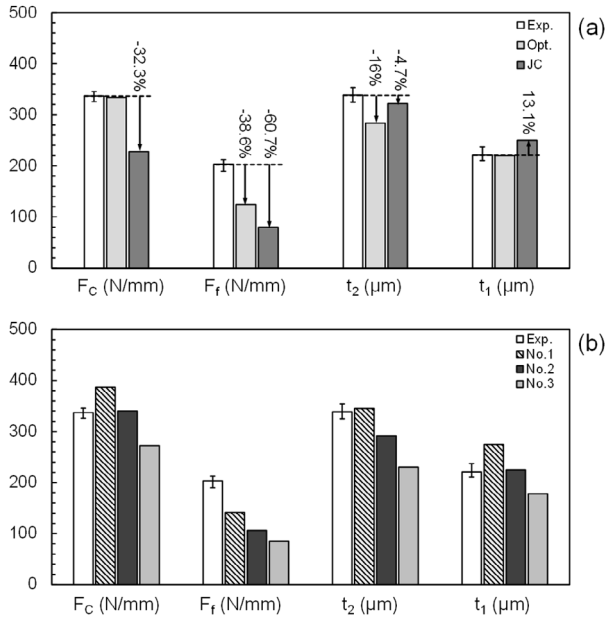

Fig. 7: (a) the comparison between the FE simulation results of forces and chip shape parameters incorporating JC and the proposed constitutive model, (b) the comparison between the experimental results and the model predictions using the parameters given in Table 2 for the proposed model (Eq. 2). V_C = 200 m/min, f = 0.016 mm/rev, 10° rake angle, VB = 0.095 mm.

Fig. 7 illustrates the cutting and feed forces as well as the t_1 and t_2 chip shape parameters along with the corresponding experimental measurements. As shown in this figure, while the difference between the simulated and measured chip parameters was nearly in the same range, around 32% and 61% error were observed in the simulated cutting and feed forces when the JC model was used. The deviations in the simulated cutting and feed forces were about 0.5% and 39% when the optimum set of material and damage parameters were used for modelling the cutting process using the proposed constitutive model.

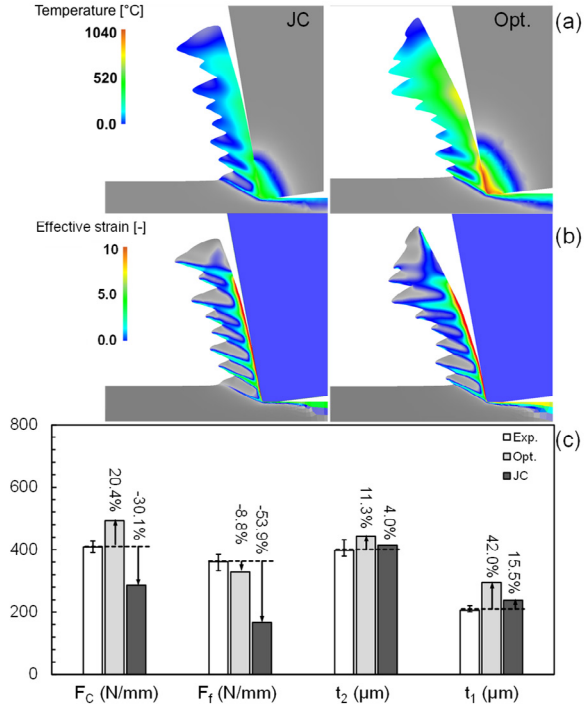

Fig. 8: (a) The comparison between the FE simulation results of temperature and (b) effective strain incorporating the JC and the proposed model in this study, (c) the comparison between the measured data and simulation results using the parameters given in Table 2 for the proposed model (Opt.) and JC model. V_C = 200 m/min, f = 0.016 mm/rev, -10° rake angle, VB = 0.142 mm.

Likewise, the FE simulation results presented in Fig. 8, for the worn tool with -10° rake angle and the flank wear land of about 0.142 mm long, showed larger deviations in feed and cutting forces when the JC model was used. However, a better agreement with the experimental results was observed for the chip shape parameters using the JC model. The underestimation in the simulated cutting and feed forces by using the JC model is also reflected in the tool-chip interface temperature, see Figs. 6 and 8a. The maximum temperature on the rake surface of the tools was about 300 °C higher when the present constitutive model with an optimum set of material and damage parameters was used for cutting simulations. It should be noted that the simulated interface temperatures incorporating the proposed constitutive model seem to agree better with the experimental temperature measurements, for example those reported by M'Saoubi and Chandrasekaran [16]. The authors measured the maximum interface temperature of about 850 °C on the rake face of coated tools (Al_2O_3 +Ti(C,N)) at the cutting speed of 180 m/min and feed rate of 0.20 mm/rev. Since the coating can potentially reduce the frictional work and it acts as a thermal barrier, the predicted maximum temperatures between 950-1050 °C seem to be more realistic than those around 650-700 °C resulted from the JC model.

The larger errors in the simulated temperature and the cutting forces indicate that the JC model fails to properly describe the flow stress properties of the work material at the relevant ranges of strain, strain rate and temperature encountered in the cutting zone. For example, as shown in Fig. 5, the JC model predicts a larger thermal softening effect than the one observed experimentally in the range between 400 °C and 900 °C. As a result, the JC model estimates lower flow stresses and thus lower heat generation and forces were obtained.

The other important observation here is the effect of strain softening term in Eq. 2 on the FE simulation results. As can be seen in Fig. 4b, all four material combinations reported for Eq.2 in Table 2 matched well with the experimental flow stress data at the low range of strains presented in Fig. 4a. The difference between these sets of material data – in three out of four cases – was only in the damage initiation criterion (W_{CL}) and the strain softening factor (n_2). However, the simulated cutting forces, chip shape parameters and temperature fields were significantly different when these sets of parameters were used for simulations, see Figs. 6 and 7. This emphasises the importance of the strain softening and the damage parameters adopted in Eq. 2 and Eq. 4 for cutting simulation of 316L austenitic stainless steel. Nevertheless, it may also be noted that, the effort here was to propose a model with the least number of material and damage parameters required for cutting simulation. Further investigations are required to incorporate a more realistic damage initiation and progression models for simulation of machining processes to improve the simulation results

6. Conclusions

In this study, a new constitutive model is proposed to describe the material hardening and softening behaviour of 316L austenitic stainless steel. A novel approach was presented for calibration of the model within the entire range of strain, strain rate and temperature encountered during the chip formation process. A significant improvement was achieved after implementation of the proposed constitutive model.

Acknowledgements

This work was partly performed under the sponsorship of the Strategic Innovation Program "Metallic Materials" (project number 2017-02517) – a joint venture of Vinnova (Sweden's Innovation Agency), Formas and the Swedish Energy Agency. The authors would also like to acknowledge the financial support of the Chalmers Area of Advance – Production and the supports received from Chalmers Centre for Metal Cutting Research. Thanks are also extended to Prof. Ragnar Larsson at Chalmers University of technology for interesting discussions.

References

[1] P. J. Arrazola, T. Özel, D. Umbrello, M. Davies, and I. S. Jawahir, "Recent advances in modelling of metal machining processes," CIRP Annals - Manufacturing Technology, vol. 62, no. 2, pp. 695-718, 2013.
[2] J. M. Rodríguez, J. M. Carbonell, and P. Jonsén, "Numerical Methods for the Modelling of Chip Formation," Archives of Computational Methods in Engineering, 2018.
[3] G. R. Johnson and W. H. Cook, "A constitutive model and data for metals subjected to large strains, high strain rates and high temperatures," in 7th International Symposium on Ballistics, The Hague, Netherlands, 1983, vol. 21, pp. 541-547: International Ballistics Committee.
[4] Y. Karpat, "Temperature dependent flow softening of titanium alloy Ti6Al4V: An investigation using finite element simulation of machining", Int. J. of Materials Processing Technology, 211, no. 4, pp. 737-749, 2011.
[5] M. Sima and T. Özel, "Modified material constitutive models for serrated chip formation simulations and experimental validation in machining of titanium alloy Ti–6Al–4V," International Journal of Machine Tools and Manufacture, vol. 50, no. 11, pp. 943-960, 2010.
[6] F. J. Zerilli and R. W. Armstrong, "Dislocation-mechanics-based constitutive relations for material dynamics calculations," Journal of Applied Physics, vol. 61, no. 5, pp. 1816-1825, 1987.
[7] A. Svoboda, D. Wedberg, and L. E. Lindgren, "Simulation of metal cutting using a physically based plasticity model," Modelling and Simulation in Materials Science and Engineering, vol. 18, no. 7, pp. 1-19, 2010.
[8] R. Liu, M. Salahshoor, S. N. Melkote, and T. Marusich, "The prediction of machined surface hardness using a new physics-based material model," Procedia CIRP, vol. 13, pp. 249-256, 2014.
[9] R. Liu, M. Salahshoor, S. N. Melkote, and T. Marusich, "A unified material model including dislocation drag and its application to simulation of orthogonal cutting of OFHC Copper," Journal of Materials Processing Technology, vol. 216, pp. 328-338, 2015.
[10] A. Malakizadi, H. Gruber, I. Sadik, and L. Nyborg, "An FEM-based approach for tool wear estimation in machining," Wear, vol. 368–369, pp. 10-24, 2016.
[11] A. Malakizadi, K. Hosseinkhani, E. Mariano, E. Ng, A. Del Prete, and L. Nyborg, "Influence of friction models on FE simulation results of orthogonal cutting process," The International Journal of Advanced Manufacturing Technology, vol. 88, no. 9, pp. 3217-3232, 2017.
[12] A. Malakizadi, S. Cedergren, I. Sadik, and L. Nyborg, "Inverse identification of flow stress in metal cutting process using Response Surface Methodology", Simulation Modelling Practice and Theory, vol. 60, pp. 40-53, 2016.
[13] D. Wedberg and L.-E. Lindgren, "Modelling flow stress of AISI 316L at high strain rates," Mechanics of Materials, vol. 91, pp. 194-207, 2015.
[14] N. Saunders, U. K. Z. Guo, X. Li, A. P. Miodownik, and J.-P. Schillé, "Using JMatPro to model materials properties and behavior," JOM, vol. 55, no. 12, pp. 60-65, 2003.
[15] H. Chandrasekaran, R. M'Saoubi, and H. Chazal, "Modelling of material flow stress in chip formation process from orthogonal milling and split Hopkinson bar tests," Machining Science and Technology, vol. 9, no. 1, pp. 131-145, 2005.
[16] R. M'Saoubi and H. Chandrasekaran, "Experimental study and modelling of tool temperature distribution in orthogonal cutting of AISI 316L and AISI 3115 steels," The International Journal of Advanced Manufacturing Technology, vol. 56, no. 9, pp. 865-877, 2011.